International Journal of Computational Methods
Vol. 16, No. 5 (2019) 1840015 (22 pages)

DOI: 10.1142/S0219876218400157

Simulations of Self-Propelled Fully Appended Ship Model at Different Speeds

Jianhua Wang, Weiwen Zhao and Decheng Wan*

State Key Laboratory of Ocean Engineering
School of Naval Architecture Ocean and Civil Engineering
Shanghai Jiao Tong University Collaborative Innovation
Center for Advanced Ship and Deep-Sea Exploration
Shanghai 200240, P. R. China
**dcwan@sjtu.edu.cn*

Received 18 December 2016
Revised 11 September 2018
Accepted 19 October 2018
Published 5 December 2018

With the great progress in supercomputers and numerical methods, the applications of computational fluid dynamics are advancing rapidly in the field of ship hydrodynamics. And the dynamic overset grid method makes it possible for computing complex ship motions. In the present work, CFD-based method coupling with dynamic overset grid technique is applied to investigate the hydrodynamic performance of the fully appended ONR Tumblehome ship model during self-propulsion condition. Open water performance of propeller and towing condition of bare hull are computed before the self-propulsion simulation. The ship model is fitted with twin rotating propellers and twin static rudders, achieving self-propulsion model point at $Fr = 0.20$ and $Fr = 0.30$, respectively. All the computations are carried out by our in-house CFD solver naoe-FOAM-SJTU, which solves the Navier–Stokes equations for unsteady turbulent flows with VOF method capturing free surface around the complex geometry models. During the self-propulsion simulation, a feedback controller is used to update the rotational speed of the propeller to achieve the target ship speed. Detailed information of the flow field during the self-propulsion condition is presented and analyzed. In addition, predicted results, i.e. self-propulsion model point, ship motions and force coefficients, are also presented and compared with the available experimental data. Good agreements are achieved, which indicates that the present approach is applicable for the self-propulsion simulation.

Keywords: Overset grid; naoe-FOAM-SJTU solver; self-propulsion; ONR Tumblehome ship.

1. Introduction

Self-propulsion is a key standard to examine a ship's powering performance and is closely bound up with energy consumption. With the coming out of energy efficiency

*Corresponding author.

design index (EEDI) proposed by International Maritime Organization (IMO), more attention is devoted to the research of ship self-propulsion character. Thus how to evaluate the self-propulsion characteristics at the design stage is of great importance and the studies in this area have been extensively progressed. However, great challenges show up with the complexity of the flow field and interaction between hull, moving rudders and rotating propellers. When dealing with the fully appended ship, the vortical structures separated from the hull and appendages can be even more complicated. Among the available approaches to perform CFD simulation of self-propulsion, direct self-propulsion simulation with discretized module of fully appended hull, rotating propeller and moving rudder is the one least reliant on geometries. Furthermore, self-propulsion requires capabilities of 6DOF motion with a hierarchy of bodies in a free surface environment. All the above aspects increase the difficulties in direct simulating the self-propulsion problems.

Up to now, the main approach for predicting self-propulsion still strongly relies on the experimental results, in which model scale experiments in a conventional towing tank account for the main part. Experimental measurements can give reliable results but conversely at high cost. Nowadays, CFD approach is becoming a powerful tool for the prediction of ship performance as numerical algorithms improve and computers gain in power. Increasing demand of high accuracy for ship self-propulsion prediction has made it essential to develop a fully coupled numerical model for the complex self-propelled ship. In addition, the dynamic overset grid method, including a hierarchy of bodies that enable computation of ship motions with moving components, makes it possible to directly compute self-propulsion with rotating propellers and turning rudders. So far, overset grid method has been successfully applied to the computations of ship hydrodynamics, especially for the simulation of hull-propeller-rudder interaction. Carrica *et al.* [2010] used a speed controller and a discretized propeller with dynamic overset grids to directly perform the self-propulsion computations. Three ship hulls were evaluated, i.e. the single-propeller KVLCC1 tanker appended with a rudder, the twin propeller fully appended surface combatant model DTMB 5613, and the KCS container ship without a rudder, and good agreements with experimental data show that direct computation of self-propelled ships is feasible. Castro *et al.* [2011] investigated the full-scale computations for self-propelled KRISO container ship KCS using discretized propeller model, and give the conclusion that the propeller operates more efficiently in full scale and is subject to smaller load fluctuations. Shen *et al.* [2015] implemented dynamic overset grid module to OpenFOAM and presented the application to the KCS self-propulsion and zigzag maneuvering simulation. Predicted results show good agreements with the experimental data, which show that the fully discretized model with overset grid method is applicable for the computations of ship hull, propeller and rudder interaction. Wang *et al.* [2016] presented the free maneuvering simulations of the ONR Tumblehome model using the overset grid method, and the predicted ship motions for the maneuvering conditions agree well with the available experimental data.

The present paper shows our recent progress in the numerical prediction of self-propulsion for fully appended ship model using dynamic overset grid method. Discretized model for rotating propellers are used in the simulation. Emphasis is put on the hydrodynamic performance for self-propulsion at different Froude numbers, i.e. $Fr = 0.20, Fr = 0.30$. The non-dimensional Froude number is defined as $Fr = U/\sqrt{gL}$, where U is the ship speed, g is gravitational acceleration and L is ship length. The main framework of this paper goes as following. The first part is the numerical methods, where naoe-FOAM-SJTU solver and overset grid method are presented. The second part is the geometry model and test conditions. Then comes the simulation part, where towing condition, open water calculation and self-propulsion will be presented systematically. In this part, extensively comparisons are performed against the experimental data including ship motions and hydrodynamic coefficients. Following this part is the numerical uncertainty study for towing condition at $Fn = 0.30$. Finally, a conclusion of this paper is drawn.

2. Numerical Methods

2.1. *Naoe-FOAM-SJTU solver*

The main framework and features of naoe-FOAM-SJTU solver are only briefly described here; detailed information can be referred to Shen *et al.* [2014, 2015], Shen and Wan [2016], Cao and Wan, [2014, 2015], Wang *et al.* [2016a, 2016b, 2017] and Zha *et al.* [2015]. The solver is based on the open source platform OpenFOAM and consists of self-developed modules, i.e. a numerical wave tank module, a full 6DOF module with a hierarchy of bodies, a mooring system module and an overset grid module. The solver has the capability of handling varies problems in naval architecture and ocean engineering, i.e. large motion response prediction for ship and platforms in ocean waves; ship resistance and seakeeping prediction; simulations of self-propulsion and free maneuvering with turning rudders and rotating propellers.

The in-house CFD code solves the Reynolds-Averaged Navier–Stokes (RANS) equations for unsteady turbulent flows around complex geometries. The unsteady RANS equations are presented as a mass conservation equation and a momentum conservation equation:

$$\nabla \cdot \boldsymbol{U} = 0 \tag{1}$$

$$\frac{\partial \rho \boldsymbol{U}}{\partial t} + \nabla \cdot (\rho \boldsymbol{U}\boldsymbol{U}) = -\nabla p_d - \boldsymbol{g} \cdot \boldsymbol{x} \nabla \rho + \nabla \cdot (\mu_{\text{eff}} \nabla \boldsymbol{U}) + (\nabla \boldsymbol{U}) \cdot \nabla \mu_{\text{eff}} + \boldsymbol{f}_\sigma, \tag{2}$$

where $\boldsymbol{U}$ is the fluid velocity, $p_d = p - \rho \boldsymbol{g} \cdot \boldsymbol{x}$ is the dynamic pressure, ρ is the mixture density of the two-phase fluid, $\boldsymbol{g}$ is the gravitational acceleration, $\mu_{\text{eff}} = \rho(\nu + \nu_t)$ is the effective dynamic viscosity, where ν and ν_t are the kinematic viscosity and kinematic eddy viscosity respectively. ν_t can be obtained by the turbulence model, which is modeled by a blended $k - \omega / k - \varepsilon$ shear stress transport (SST) model. $\boldsymbol{f}_\sigma$ is the source term for surface tension.

Near wall treatment adopts wall functions, which is based on the law of the wall and requires the $y+$ of the first cell outside the walls is in the log-layer, which starts at about $y+30$ and, depending on the Reynold number, extends up to say $y+200$. Therefore, this approach can reduce computational grid with coarse layer near the ship. The viscous sublayer ($y+ < 5$) and buffer layer ($5 < y+ < 30$) is located in the first cell and the velocity distribution can be approximate according to the law within the cell. Detailed information of wall functions can be referred to Pope [2000].

Free surface is captured by a VOF approach with bounded compression technique [Berberović *et al.* (2009)] and the transport equation is expressed as:

$$\frac{\partial \alpha}{\partial t} + \nabla \cdot [(\boldsymbol{U} - \boldsymbol{U_g})\alpha] + \nabla \cdot [\boldsymbol{U_r}(1-\alpha)\alpha] = 0, \tag{3}$$

where α is volume of fraction, 0 and 1 represent air and water respectively and $0 < \alpha < 1$ stands for the interface between two-phase fluid. $\boldsymbol{U_r}$ is the velocity field used to sharpen the interface while the "$\nabla\cdot$" guarantees conservation and $(1-\alpha)\alpha$ guarantees boundedness.

The merged PISO-SIMPLE (PIMPLE) algorithm is applied to solve the coupled equations for velocity and pressure field. The semi-implicit method for pressure-linked equations (SIMPLE) algorithm allows to couple the Navier–Stokes equations with an iterative procedure. And the pressure implicit splitting operator (PISO) algorithm enables the PIMPLE algorithm to do the pressure-velocity correction. Detailed description for the SIMPLE and PISO algorithm can be found in Ferziger and Peric [1999] and Issa [1986]. In addition, several built-in numerical schemes in OpenFOAM are used in discretizing and solving the partial differential equations (PDE). The convection terms are discretized by a second-order TVD limited linear scheme, and the diffusion terms are approximated by a second-order central difference scheme. An implicit Euler scheme is used for temporal discretization.

2.2. *Overset grid method*

The overset grid method is of great importance for direct simulating the full coupled hull, propeller and rudder system. Here a brief introduction for the utilization of overset grid module in naoe-FOAM-SJTU solver is presented. Overset grid is a grid system that made up of blocks of overlapping structured or unstructured grids. By using dynamic overset grid technique, the overlapping grids can move independently without any constraints. To this aim, the cells in the computational domain are classified into several types, i.e. fringe, hole, donor, etc. The information of cell types is stored in the domain connectivity information (DCI) file. In our present solver, Suggar++ [Noack *et al.* (2009)] is utilized to generate the domain connectivity information (DCI) for the overset grid interpolation. To combine OpenFOAM with Suggar++, a communication, which is responsible for DCI exchange between OpenFOAM and Suggar++, has been implemented using the Message Passing Interface (MPI) library [Shen *et al.* (2015)]. Other features consist of a full 6DOF motion

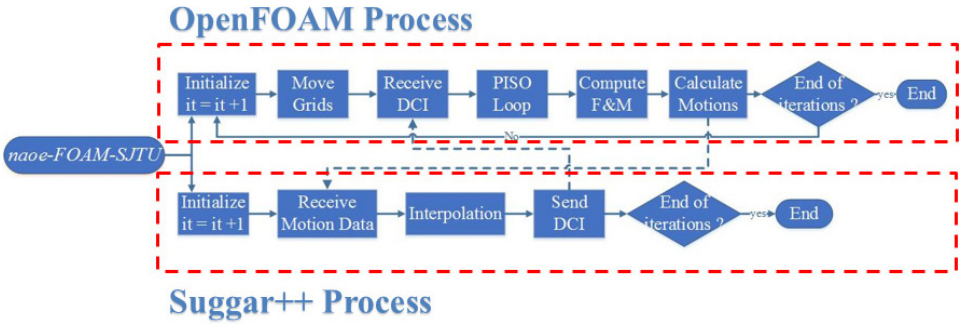

Fig. 1. Flowchart of the parallel calculation procedure.

module with a hierarchy moving components and several modifications for sparse matrix solvers and MULES solver to excluded non-active cells. The flowchart of the parallel calculation between OpenFOAM processor and Suggar++ processor is shown in Fig. 1. During the computation, the OpenFOAM processors are used to calculate the flow field, where the DCI need to be received from the Suggar++ process in order to solver the constructed equations. Within the flow calculation procedure, the forces and motions will be obtained and the motion data will then be delivered to the Suggar++ process to calculate the DCI for the next time step.

By using overset grid method, the full 6DOF motion solver allows the ship and its appendages as well as the moving components to move simultaneously. Two coordinate systems are used to solve the 6DOF equations. One is the inertial system (earth-fixed system) and the other is non-inertial system (ship-fixed system). The inertial system can be fixed to earth or move at a constant speed with respect to the ship. The non-inertial system is fixed to the ship and can translate or rotate according to the ship motions. More information of the 6DOF motion solver with overset grid module implementation can be followed Shen *et al.* [2015]. In our present study, the computational domain is decomposed into several overlapping grids, where each moving component has its own grid to deal with complex motion problems.

3. Geometry Model and Test Conditions

3.1. *Geometry model*

The present numerical simulations are carried out for the ONR Tumblehome model 5613, which is a preliminary design of a modern surface combatant fully appended with skeg and bilge keels. The ship model also involves rudders, shafts and propellers with propeller shaft brackets. The geometry model of ONR Tumblehome without propellers and shaft brackets is shown in Fig. 2, and its principle parameters are listed in Table 1. The ship model is used as one of the benchmark cases in Tokyo 2015 CFD workshop in ship hydrodynamics [Tokyo (2015)]. Experiments were widely performed at Iowa Institute of Hydraulic Research (IIHR) wave basin for this ship

Fig. 2. Geometry model of ONR Tumblehome ship.

Table 1. Principle dimensions of fully appended ship.

Main particulars		Model scale	Full scale
Length of waterline	$L_{WL}(m)$	3.147	154.0
Maximum beam of waterline	$B_{WL}(m)$	0.384	18.78
Depth	$D(m)$	0.266	14.50
Draft	$T(m)$	0.112	5.494
Displacement	$\Delta(kg)$	72.6	8.507e6
Wetted surface area (fully appended)	$S_0(m^2)$	1.5	NA
Block coefficient (CB)	$\nabla/(L_{WL}B_{WL}T)$	0.535	0.535
LCB	$aft.of FP(m)$	1.625	NA
Vertical center of gravity (from keel)	$KG(m)$	0.156	NA
Metacentric height	$GM(m)$	0.0422	NA
Moment of inertia	K_{xx}/B_{WL}	0.444	0.444
	$K_{yy}/L_{WL}K_{zz}/L_{WL}$	0.246	0.25
Propeller diameter	$D_P(m)$	0.1066	NA
Propeller shaft angle (downward pos.)	$\varepsilon(^\circ)$	5	NA
Propeller rotation direction (from stern)		inward	inward

model and the available experimental data can be used to validate our present computational results.

3.2. *Test conditions*

The present work is for self-propulsion computation of ONR Tumblehome ship model. According to the experimental setup, the fully appended ship is set to advance at model point in calm water with twin rotating propellers and rudders. In the present simulation, two approaching speeds, i.e. $U = 1.110\,\mathrm{m/s}$ and $U = 1.667\,\mathrm{m/s}$, corresponding to Froude number of $Fr = 0.20$ and $Fr = 0.30$, are taken into account to further investigate the self-propulsion performance of the fully appended ONR Tumblehome model. Fully unstructured grids used in this paper are generated by *snappyHexMesh* with the background grid generated by *blockMesh*, both are pre-processing utilities provided by OpenFOAM. Furthermore, both self-propelled simulations are performed with the same overlapping grids.

4. Simulation Procedure and Results

The simulation procedure for self-propulsion includes three parts, first is the towing ship condition, where the final solution can be mapped as the initial state for the self-propulsion computation. This pre-processing step can save large amount of

computational time by starting with a developed flow field and boundary layer. The second part is the open water calculation for the propeller, and this step can give the open water characteristics for the propeller. The final process is to calculate the self-propelled ship model, where the initial ship speed is set to the target cruise speed and a feedback proportional-integral (PI) controller is applied to adjust the rotational rate of the propeller to achieve the desired ship speed.

4.1. *Towing condition*

The simulation of towing condition is followed by the experimental setup, and the advancing speeds are $U = 1.110\,\text{m/s}$ and $U = 1.667\,\text{m/s}$, corresponding to $Fr = 0.20$ and $Fr = 0.30$. The computations are carried out without appendages and moving components. Overset grid approach is applied in this simulation, and the computational domain is separated into the hull grid and background grid (Fig. 3). For the towing condition computation, the background domain extends to $-1.5L_{pp} < x < 5.0L_{pp}$, $-1.5L_{pp} < y < 1.5L_{pp}$, $-1.0L_{pp} < z < 0.5L_{pp}$, and the hull domain has a much smaller region with a range of $-0.15L_{pp} < x < 1.2L_{pp}$, $-0.13L_{pp} < y < 0.13L_{pp}$, $-0.2L_{pp} < z < 0.2L_{pp}$. The total grid number is 1.87 M, with 0.82 M for hull grid and 1.05 M for background grid. Boundary conditions are identical with zero velocity and zero gradient of pressure imposed on inlet and far-field boundaries, while a pressure outlet boundary condition is applied for the outlet boundary.

During the computation, the ship model is advancing at the desired speed while the remaining 5 freedoms of degree are constrained. Through this way, the calculated flow field can be used as an initial state for the self-propulsion simulation. Cook [2011] investigated the appendages effect on the total resistance for ONR Tumblehome model at different Froude numbers, and the comparison between the present

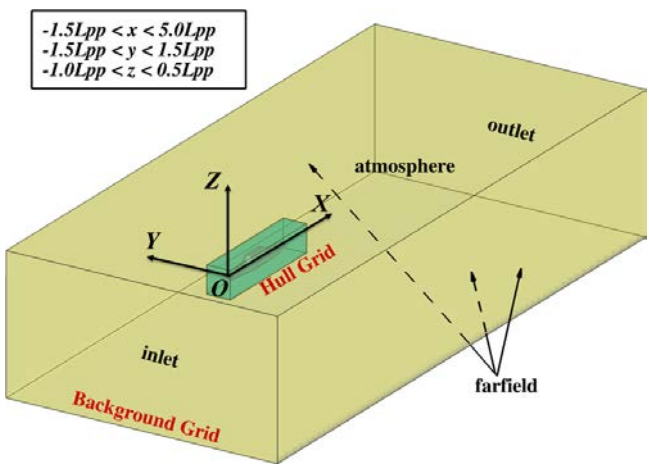

Fig. 3. Computational domain for towing condition.

Table 2. Total resistance comparison with bare hull simulation.

Fr	EFD (IIHR) fully appended	EFD (INSEAN) bare hull w/o BK	CFD (IIHR) bare hull w/o BK	CFD (Present) bare hull w/o BK
0.20	$4.54N$	-18.6%	-15.7%	-17.9%
0.30	$11.30N$	-19.0%	-20.8%	-18.3%

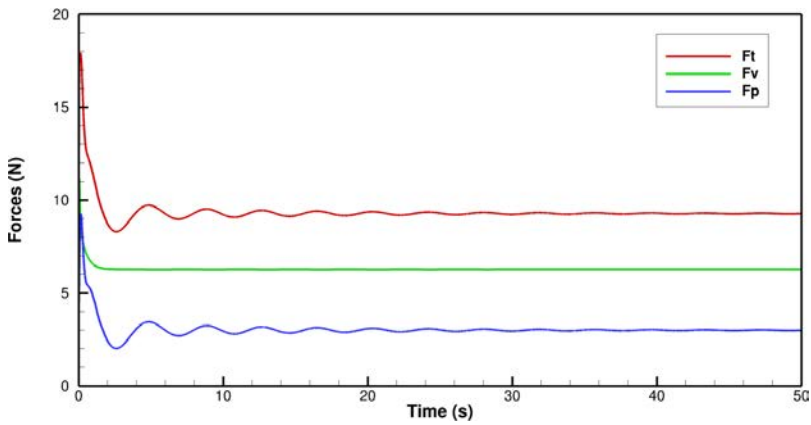

Fig. 4. Time histories of the ship resistance at $Fr = 0.3$.

numerical results and the experimental data as well as CFD results by IIHR are listed in Table 2. An obvious phenomenon can be observed from the table that the total resistance of bare hull without bilge keels is much smaller than the fully appended model. The present results for the bare hull resistance show good agreement with the EFD data performed at INSEAN and the CFD results from IIHR. Figure 4 shows the convergence curves of the three components of ship resistance at $Fr = 0.30$ in 50 s, where Ft, Fv and Fp stands for total force, viscous force and pressure force, respectively. Satisfactory agreements for the towing condition are achieved and high accuracy result can give a better initial state of the self-propulsion simulation. In addition, to further validate our numerical results, grid uncertainty analysis is performed for the towing condition, which will be discussed in the grid uncertainty analysis part later.

4.2. *Open water calculations*

In the present study, open water curves are obtained by the single-run procedure described in Xing *et al.* [2008]. As for the single-run procedure, the propeller is towing at a small acceleration to fulfil a wide range of advancing velocities in one turn. Based on overset grid, the computational domain is separated into two parts, i.e. background grid and propeller grid (Fig. 5(a)). When doing the calculation, the propeller grid rotates with the rotating propeller while the background grid moves

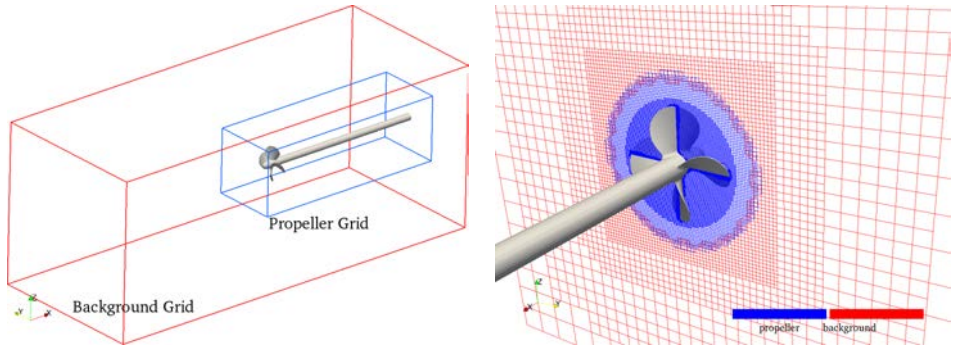

(a) Computational domain (b) Grid distribution around propeller

Fig. 5. Computational domain and grid distribution for open water calculation.

forward with the propeller advancing velocity. The total number of the computational grids is 1.13 M with 0.51 M for propeller grid and 0.62 M for background grid. The grid distribution around propeller disk is shown in Fig. 5(b). Calculated open water curves are compared to the experimental results performed by IIHR [available at Tokyo 2015 CFD Workshop (2015)]. The comparison between the numerical results and experimental data can be used to validate the current dynamic overset grid method coupled with single-run approach in simulating rotating propellers.

During the procedure, the rotational speed of propeller is set to fixed value $n = 8.97\,\mathrm{r/s}$ according to the test model point for self-propulsion at $Fr = 0.20$. Note that open water curves can be obtained by different rotating speed of propeller using single-run approach, and here we use the model point at $Fr = 0.20$ with the consideration of larger time step can be applied at low speed of propeller. Large range of advancing speed is performed to achieve the desired advance coefficient J. Thrust coefficients K_T, torque coefficient K_Q and η_0 efficiency for each advance coefficient are obtained from the calculated thrust and torque. The propulsive coefficients mentioned above are defined as:

$$J = \frac{V_A}{nD_P}, \tag{4}$$

$$K_T = \frac{T}{\rho n^2 D_P^4}, \tag{5}$$

$$K_Q = \frac{Q}{\rho n^2 D_P^5}, \tag{6}$$

$$\eta_0 = \frac{JK_T}{2\pi K_Q}, \tag{7}$$

where T and Q are the propeller thrust and torque, D_P is the diameter of propeller, n is the rotational speed of propeller represented by resolution per second (RPS) and V_A is the advancing speed. The propeller accelerates from $V_A = 0\,\mathrm{m/s}$ to

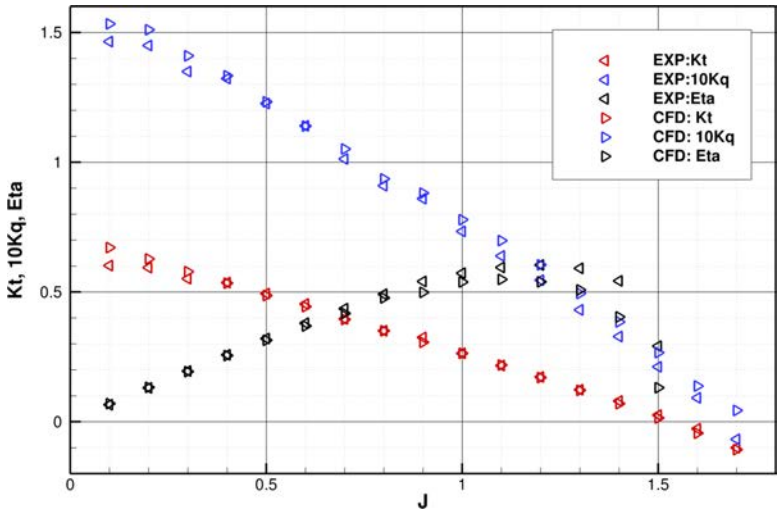

Fig. 6. Open water results by experiment (left triangle) and CFD (right triangle).

$V_A = 1.721\,\text{m/s}$ in 10 seconds with advance coefficient various from $J = 0$ to $J = 1.8$. The predicted results of the open water curves are shown in Fig. 6 and overall agreement is achieved according to the comparison with the experiment. However, the numerical results for torque coefficient K_Q and thrust coefficient K_T are not so good at both the beginning and the end. Fig. 7 shows the vortical structures using iso-surface of $Q = 200$ and colored by the axial velocity at three advancing coefficients, i.e. $J = 0.9, J = 1.0$ and $J = 1.1$. Tip vortices of the propeller are resolved clearly, and a decreasing with the strength of vortices is experienced with

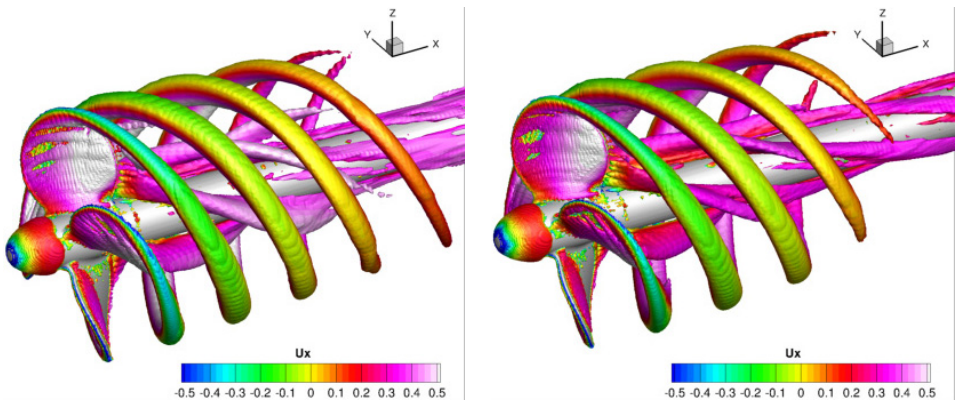

(a) $J = 0.9$ (b) $J = 1.0$

Fig. 7. Isosurfaces of $Q = 200$ at different advance coefficients colored by axial velocity.

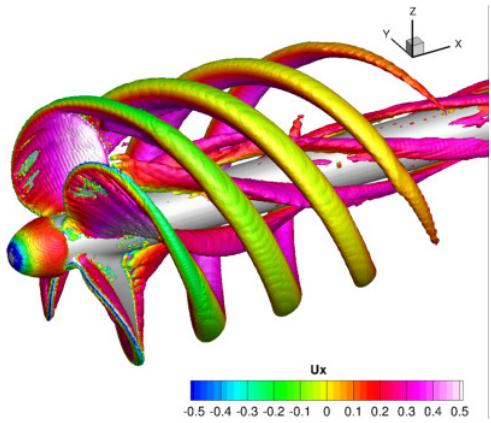

(c) $J = 1.1$

Fig. 7. (*Continued*)

the increasing of advance coefficient. This phenomenon is mainly due to the angle of attack decreases when the advance coefficient becomes larger.

The hub vortices of the propeller experienced the same trend with the strength decreasing. With rather coarse mesh and the RANS turbulence model, the evolution of vortical structures is relatively stable. In spite of the limitation of RANS model, the calculated coefficients K_T, K_Q and η_0 show overall agreement with the experimental data by the present dynamic overset grid method coupled with single-run approach.

4.3. *Self-propulsion simulation*

As mentioned in test conditions, two approaching speeds, i.e. $U = 1.110\,\text{m/s}$, $U = 1.667\,\text{m/s}$, are performed for the self-propulsion simulation. The former situation is one of the benchmark cases (Case 3.9) in Tokyo 2015 Workshop on CFD in ship hydrodynamics [2015]. And the experiment data for the latter one is also available in Elshiekh [2014]. According to the experimental setup, the fully appended ship is set to approaching at model point in calm water. The twin rotating propellers, updating RPS by a feedback PI controller, provide the thrust for the ship to move forward. The proportional and integral constants were set to 800 with the consideration of large PI constants can accelerate the convergence of the propeller revolution rate and reduce the total computation time.

Using dynamic overset grid technique, here we have four parts of the computational grids, i.e. grid around ship hull, propeller grid, rudder grid and background grid. Background grid is the root element during the hole-cutting procedure, and the hull grid is at parent motion level with children grid of twin propellers and rudders. The four grid blocks have overlapping areas, which can move independently without restrictions and build connections among them by interpolation at appropriate cells

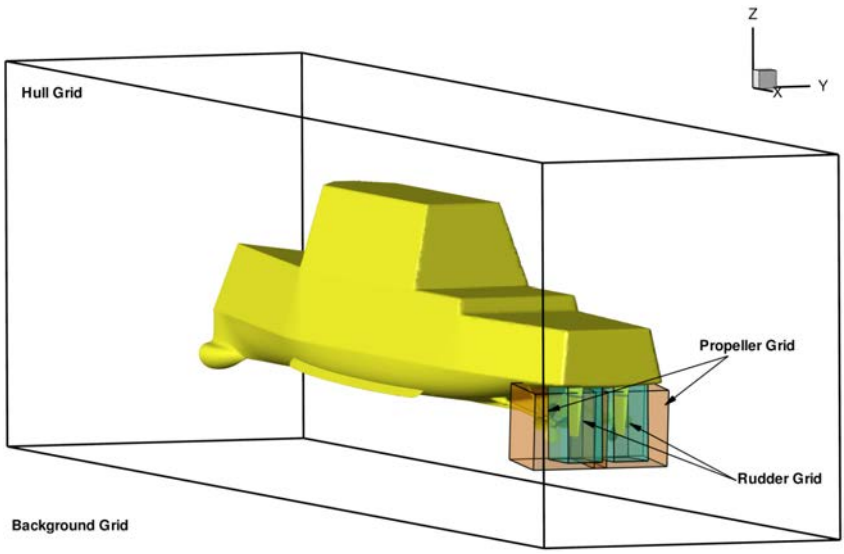

Fig. 8. Overset grid arrangement for self-propulsion simulation.

Table 3. Grid distribution in each part.

Grid	Total	Port	Starboard	Level
Background	1.34 M	NA	NA	Root
Hull	2.61 M	NA	NA	Parent
Propeller	2.28 M	1.14 M	1.14 M	Children
Rudder	0.58 M	0.29 M	0.29 M	Children
Total	6.81 M	NA	NA	NA

or points. The computational domain is the same as the towing condition and the overset grid arrangement for the self-propulsion simulation is shown in Fig. 8.

The total grid number for the self-propulsion simulation is 6.81 M and the detailed grid information in each part is shown in Table 3. Considering the grid quality in overlapping areas, several refinement regions are applied to offer enough donor cells for interpolation. Grids in gaps should be handled specifically to make sure that the grid dimensions of different grid blocks in overlapping areas are similar. Good grid quality at overlapping areas can resolve better flow information and reduce the computational cost. The global and local grid distribution around ship hull is shown in Fig. 9.

The initial state of the self-propulsion simulation is obtained by interpolating data from the final flow field of towing condition to accelerate the convergence of the calculation. The interpolation is conducted by the *mapFields* utility, which is a preprocessing tool supported by OpenFOAM. During the self-propulsion simulation, the twin propellers start from static state and speed up the rotational velocity to

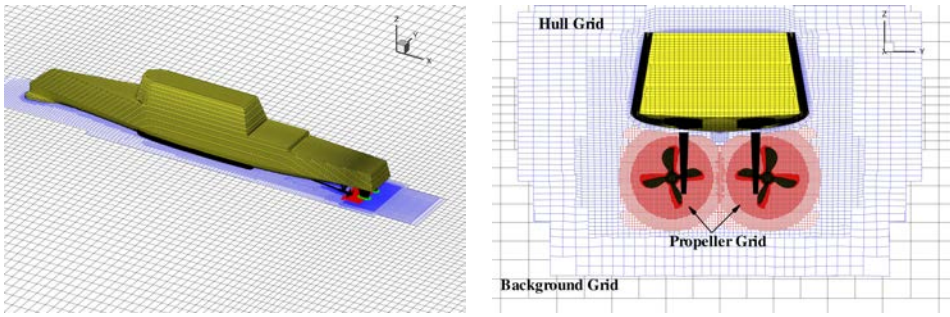

(a) Global view (b) Local view

Fig. 9. Grid distribution around ship hull.

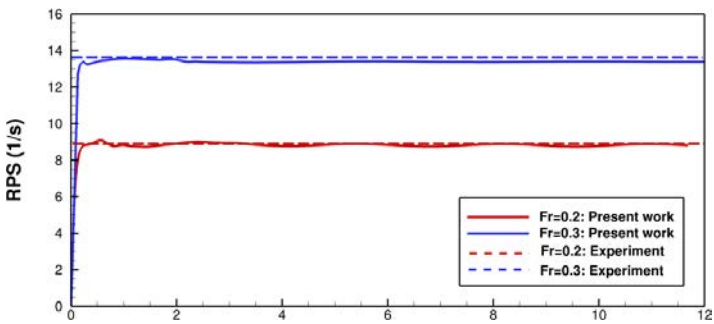

(a) RPS

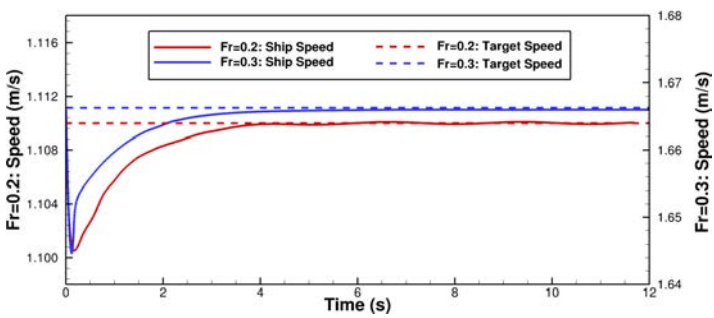

(b) Ship speed

Fig. 10. Time histories of RPS and ship speed.

provide enough thrust. The time histories of the rotational speed of propellers and ship model advancing speed for both conditions are shown in Fig. 10.

Both time histories of the RPS start from zero and increase quickly and the curves of the RPS converge to the desired the value in about 5 s at model scale. According to Fig. 10(b), the ship speed first decreases due to less thrust provided

by the rotational propellers and with the increasing RPS of propellers, the available thrust can prompt the ship speed comes back to the target value. In addition, the time histories of ship speed describe the characters at the beginning of different conditions, where the increasing rate of speed as well as the speed loss for $Fr = 0.30$ are larger than that of $Fr = 0.20$. This is mainly due to the fact that larger target speed requires larger thrust, thus more speed loss at beginning with static propeller and larger increasing rate with higher RPS of propeller. Figure 10 also presents the test results for the rotational speed of propeller and target ship speed. Numerical results of both RPS and ship speed can finally achieve a stable desiring state.

Table 4 lists the numerical results of self-propulsion model point, ship motions as well as self-propulsion coefficients. All the predicted force coefficients are in non-dimensional format using the provided wetted surface area at rest S_0, fluid density ρ and ship advancing speed U. The force coefficients are defined as follows:

$$C_T = \frac{F_T}{\frac{1}{2}\rho U^2 S_0}, \tag{8}$$

$$C_V = \frac{F_V}{\frac{1}{2}\rho U^2 S_0}, \tag{9}$$

$$C_P = \frac{F_P}{\frac{1}{2}\rho U^2 S_0}, \tag{10}$$

Note that the computation is carried out to predict the self-propulsion model point and the propulsion coefficients are obtained by the predicted results, none of the coefficients except n can be compared with the measured data. So only parts of the results are compared with the experiment. Table 4 gives a general comparison for ship motions and force coefficients. It shows that the present CFD approach can precisely achieve the desired ship speed and the computational results of ship motions can also give a general performance compared with the experiments. The

Table 4. Numerical results for ship motions and self-propulsion coefficients.

	$Fr = 0.20$			$Fr = 0.30$		
Parameters	CFD	EFD*	Error	CFD	EFD*	Error
u (m/s)	1.109	1.125	−1.4%	1.664	1.667	−0.2%
sinkage$\sigma \times 10^2$(m)	$2.41E{-}1$	$2.26E{-}1$	6.5%	$5.78E{-}1$		
trimτ (deg)	$4.64E{-}2$	$3.86E{-}2$	20.3%	$7.81E{-}2$		
$C_T \times 10^3$	5.291			5.465		
$C_V \times 10^3$	3.752			2.155		
$C_P \times 10^3$	1.539			3.310		
$n(RPS)$	8.819	8.97	−1.7%	13.389	13.684	−2.16%
K_T	0.242			0.246		
K_Q	0.616			0.673		

Note: *The sinkage and trim of experimental data at $Fr = 0.20$ is available at Tokyo 2015 CFD Workshop [2015] and is not available for $Fr = 0.30$, so only numerical results are presented.

sinkage and trim are larger in high Froude number, while the thrust coefficient K_T and torque coefficient K_Q are at the same level. In addition, according to the simulated force coefficients, the viscous coefficient C_F accounts for the main part of the total resistance at $Fr = 0.20$, while the pressure coefficient C_P occupies

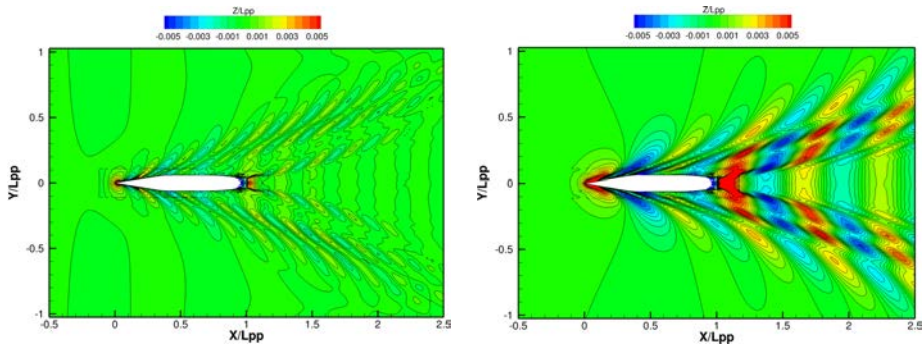

(a) $Fr = 0.20$ (b) $Fr = 0.30$

Fig. 11. Wave patterns at different Froude number colored by non-dimensional wave height Z/L_{pp}.

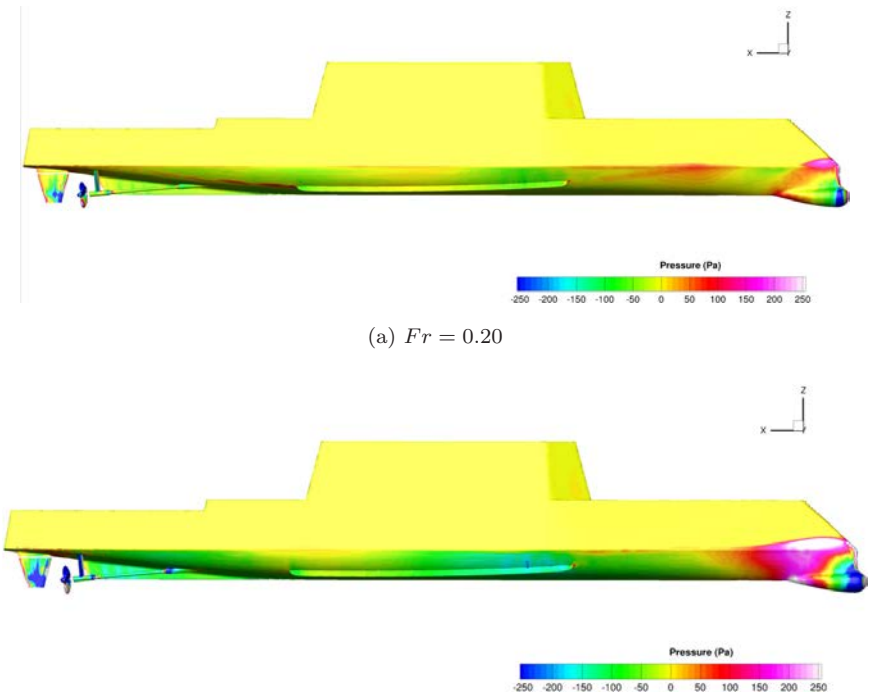

(a) $Fr = 0.20$

(b) $Fr = 0.30$

Fig. 12. Pressure distribution around ship hull, propellers and rudders.

a dominant place at $Fr = 0.30$. This further confirms that pressure effect, which is also called the wave-making resistance, plays an important role at high Froude numbers, especially when $Fr > 0.30$.

The rotational speed of the propeller n (model point) computed by our own solver naoe-FOAM-SJTU is 8.819 and 13.389 for $Fr = 0.20$ and $Fr = 0.30$, respectively. Both results are underestimated within 3% compared with the experimental data. The high accuracy of the predicted rotational speed of propeller confirms that the present dynamic overset grid approach is applicable to predict the model point for free running ship model.

Figure 11 shows the wave patterns for self-propulsion at different conditions. The flow region and velocities are non-dimensioned by the ship model length L_{WL} and magnitude velocity U. Both the wave height and wave length at $Fr = 0.30$ is significantly larger. Pressure distribution around ship hull, twin propellers and rudders is shown in Fig. 12. The distribution at different Froude number has a

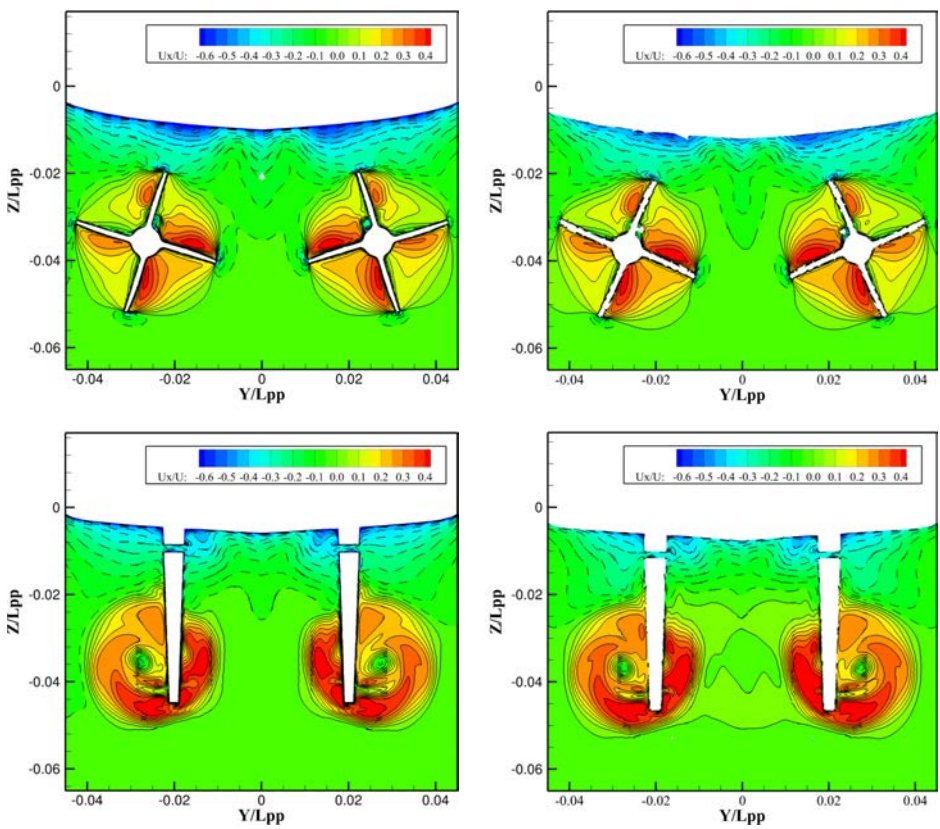

(a) $Fr = 0.20$ (b) $Fr = 0.30$

Fig. 13. Wake distribution at different Froude number (upper for slice $X/L_{pp} = 0.909$/propeller disk; lower for slice $X/L_{pp} = 0.965$/rudder).

consistent relationship to the wave patterns. Larger bow wave results in larger pressure in the forehead of the ship hull. As for the pressure distribution around the twin propellers and rudders, pressure distribution experience the same trend with the bow pressure. This is mainly due to the higher rotating speed at $Fr = 0.30$.

Figure 13 presents the detailed flow information at wake region, i.e. propeller disk ($X/L_{pp} = 0.909$) and the rudder section ($X/L_{pp} = 0.965$). From the figure we can see that the boundary layer around ship hull at high Froude number is thinner and the non-dimensional axial velocity is approximately the same, which can further explain the thrust coefficients are at the same level in different conditions. Little discrepancy is found for the wake distribution at the rudder section due to different vortex strength, which will be described later.

Figure 14 shows a profile view of vortical structures displayed as isosurface of $Q = 200$ colored by axial velocity. According to the stern view of the vortical structure, tip vortices of the propellers are clearly resolved even when passing through the rudders, but dissipate quickly within the coarser mesh downstream. In addition, the strength of tip vortices is stronger in higher Froude number, which can be clearly seen in the figure. The hub vortex observed is stronger and has a much larger size so that it is still somewhat resolved by the coarser grid downstream of the refinement. Another obvious phenomenon can be seen from the figure is that

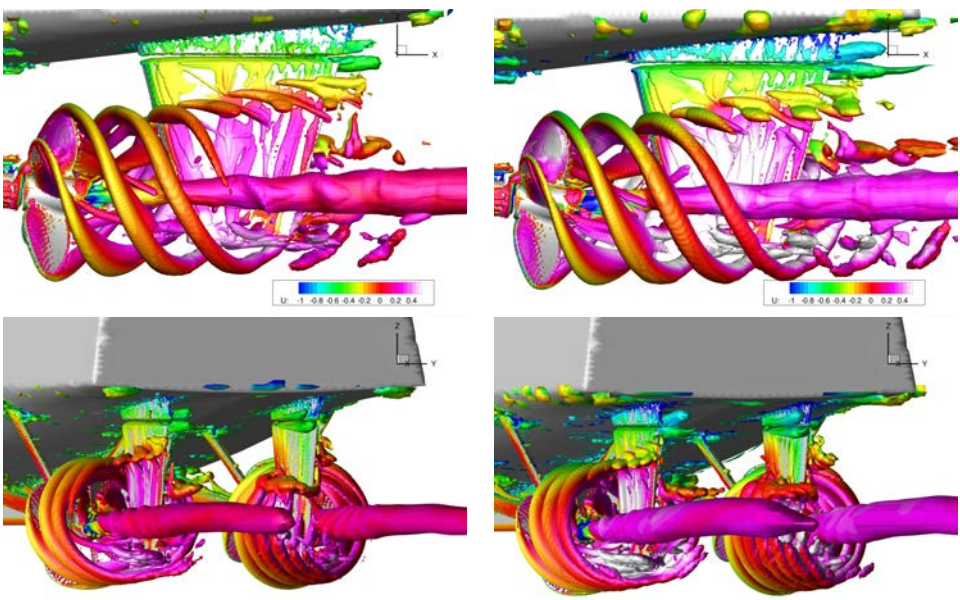

(a) $Fr = 0.20$ (b) $Fr = 0.30$

Fig. 14. Profile and 3D view of vortical structures around twin propellers and rudders.

the vortices after the rudder root, which is caused by the artificial gap between the rudder and rudder root.

Figure 14 also shows the 3D view of vortical structure, where strong interaction between the propeller vortex and the rudder geometry is occurred. The strong hub vortex of the propeller is rarely affected by the following rudder, which is due to the fact that the axis of the rudder is not aligned with the axis of propeller. An interesting effect occurs when the tip vortices of blades pass through the rudders, where the vortices are strongly affected by the rudder geometry both at the inward and outward side. In addition, little flow interaction is observed between the port side propeller and starboard side propeller (Figs. 13 and 14). Furthermore, the strength of the hub vortex in higher Froude number is also stronger than the lower one at the same grid size. The strong flow interaction between the propellers and rudders can result in complex hydrodynamic performance of ship hull.

5. Numerical Uncertainty Analysis

Estimating uncertainties in simulation results from CFD codes is essential to prove its reliability. However, with the fact of the large amount of computing time required by the self-propulsion, grid uncertainty analysis is only conducted on the towing condition in the present work with consideration of the simplicity of the overset grid arrangement in towing condition for bare hull calculation (only two part of grid is applied).

Grid uncertainty study in the present work follows the verification methodology described in Stern *et al.* [2006]. The grid convergence solution (R_G) of the different solutions (S_i, at least three) is defined as:

$$R_G = \frac{S_2 - S_1}{S_3 - S_2} \tag{11}$$

where $S_i, i = 1, 2, 3$, correspond to solutions with fine, medium, and coarse case, respectively. Three convergence conditions are possible:

$$\begin{aligned} &\text{(i)} \quad 0 < R_G < 1 \quad Monotonicconvergence \\ &\text{(ii)} \quad R_G < 0 \quad Oscillatoryconvergence \\ &\text{(iii)} \quad R_G > 1 \quad Divergence \end{aligned} \tag{12}$$

For condition (i), generalized Richardson extrapolation (RE) is used to estimate grid uncertainty U_G. For condition (ii), uncertainties are estimated simply by attempting to bound the error based on oscillation maximums S_U and minimum S_L, i.e. $U_G = 1/2(S_U - S_L)$. While for condition (iii), errors and uncertainties cannot be estimated.

The grid uncertainty study is carried out for towing condition with bare hull model at $Fr = 0.30$. Three grids with a refinement ratio of $\sqrt{2}$ in each direction are performed. Considering the grids used in the present calculation are fully

Table 5. Grid uncertainty results for towing condition at $Fr = 0.30$.

Parameters	ID	Grid Size (M)	$C_P(10^{-3})$	$C_V(10^{-3})$	$C_T(10^{-3})$	Error
EFD					4.639	
Fine	S_1	3.65	3.098	1.549	4.647	0.17%
Medium	S_2	1.87	3.076	1.503	4.579	−1.29%
Coarse	S_3	0.68	3.124	1.690	4.814	3.77%
R_G			−0.458	−0.246	−0.289	
$U_G(\%S_2)$			4.226	4.691	1.824	
Convergence type			Oscillatory	Oscillatory	Oscillatory	

Table 6. Predicted force coefficients for different time step.

Time step (ms)	$C_P(10^{-3})$	$C_V(10^{-3})$	$C_T(10^{-3})$	Error
			4.639	
0.5	3.093	1.494	4.587	−1.12%
1.0	3.076	1.503	4.579	−1.29%
1.5	3.054	1.513	4.567	−1.55%

unstructured, the systematic refinement in three directions is very difficult. In order to do the grid uncertainty study, an alternative approach is applied as follows. The background grid required by the *snappyHexMesh* is refined by splitting cells. Three systematic background grids with specified refinement ratio are taken into account. The final generated grids are approximately refined (not exactly the same) according to the grid convergence study. The results of the grid uncertainty is listed in Table 5.

The force coefficients, i.e. C_P, C_V, and C_T, are used to estimate the grid uncertainty of the towing condition. The results have good convergence as shown in Table 5. All coefficients show oscillatory convergence with R_G of $-0.458, -0.246$, and -0.289, respectively. The C_V meets the maximum grid uncertainty with $U_G = 4.691\%$ and the grid uncertainty of total resistance coefficient C_T is only 1.824%, which confirms that the grid density has limited effect on the resistance in the current range of grid size.

In addition, time step sensitivity study is conducted for the medium grid case with three different time steps, i.e. $\Delta t = 0.0005\,\text{s}$, $\Delta t = 0.001\,\text{s}$ and $\Delta t = 0.0015\,\text{s}$. The predicted results of the force coefficients for different time step are shown in Table 6.

It is obvious that the difference of force coefficients predicted at different time steps in not significantly. It should be noted that the time step used for towing condition is 1.5 ms, while a smaller time step of 0.5 ms is applied for the simulation of self-propulsion. The present time step sensitivity study proved that the simulation results is reliable for medium grid with the specified time step.

6. Conclusion

This paper presents the self-propulsion simulations of fully appended ONR Tumblehome at two different speeds, i.e. $Fr = 0.20, Fr = 0.30$. All the simulations are performed using in-house CFD solver naoe-FOAM-SJTU. During the simulation, the moving objects are handled by the dynamic overset grid method, and a feedback proportional–integral (PI) controller is employed to adjust the rotational speed of the propeller to achieve the desired ship speed.

Towing condition for bare hull model at different Froude numbers are carried out to give an approximate initial state of the self-propulsion computation. Predicted total resistance are compared with the experimental results and satisfactory agreement is achieved. Furthermore, grid uncertainty analysis and time step sensitivity study are performed with the bare hull towing condition at $Fr = 0.30$. The predicted force coefficients show oscillatory convergence and the grid uncertainty of C_T is 1.824%, indicating that the grid density has limited effect on the resistance in the current range of grid size. Predicted results are less dependent on the different time steps varies from 0.5 ms to 1.5 ms. Open water calculations are also carried out beforehand using the single-run method and the numerical results show an overall agreement with the experiment performed at IIHR.

The time histories of RPS and ship speed are converged to the target value in about 5 s, and the increasing rate of speed as well as the speed loss for $Fr = 0.30$ is larger than that of $Fr = 0.20$. In addition, according to the simulated force coefficients, the viscous coefficient C_V accounts for the main part of the total resistance at $Fr = 0.20$, while the pressure coefficient C_P occupies a dominant place at, which further confirms that pressure effect plays an important role with high Froude number, especially when $Fr > 0.30$. Predicted model point at different Froude number of self-propulsion simulation are underestimated by 1.7% and 2.16%, respectively. Detailed information of the flow field around twin propellers and rudders, i.e. wave patterns, wake distribution, pressure distribution, and vortical structures, at different Froude numbers are depicted and analyzed to explain the strong interaction among the ship hull, propellers and rudders.

Future work will focus on self-propulsion simulation in waves. Difficulties will be the complex phenomena of moving propellers with large ship motions. More work will be done to do the free maneuvering simulation depending on the computed self-propulsion results.

Acknowledgments

This work is supported by the National Natural Science Foundation of China (51879159, 51490675, 11432009, 51579145), Chang Jiang Scholars Program (T2014099), Shanghai Excellent Academic Leaders Program (17XD1402300), Program for Professor of Special Appointment (Eastern Scholar) at Shanghai Institutions of Higher Learning (2013022), Innovative Special Project of Numerical Tank of Ministry of Industry and Information Technology of China (2016-23/09) and

Lloyd's Register Foundation for doctoral student, to which the authors are most grateful.

References

Berberović, E., van Hinsberg, N., Jakirlić, S., Roisman, I. and Tropea, C. [2009] "Drop impact onto a liquid layer of finite thickness: Dynamics of the cavity evolution," *Phys. Rev.* **79**, 36306.

Cao, H. and Wan, D. [2014] "Development of multidirectional nonlinear numerical wave tank by naoe-FOAM-SJTU solver," *Int. J. Ocean Syst. Eng.* **4**, 52–59.

Cao, H. and Wan, D. [2015] "RANS-VOF solver for solitary wave run-up on a circular cylinder," *China Ocean Eng.* **29**, 183–196.

Carrica, P. M., Castro, A. M. and Stern, F. [2010] "Self-propulsion computations using a speed controller and a discretized propeller with dynamic overset grids," *J. Marine Sci. Technol.* **15**, 316–330.

Castro, A. M., Carrica, P. M. and Stern, F. [2011] "Full scale self-propulsion computations using discretized propeller for the KRISO container ship KCS," *Comput. Fluids* **51**, 35–47.

Cook, S. S. [2011] "Effects of headwinds on towing tank resistance and PMM tests for ONR Tumblehome," Master Thesis, The University of IOWA.

Elshiekh, H. [2014] "Maneuvering characteristics in calm water and regular waves for ONR Tumblehome," Master Thesis, The University of IOWA.

Ferziger, J. H. and Peric, M. [2012] "Computational methods for fluid dynamics," *Springer Science & Business Media*, 3rd revised edition.

Issa, R. I. [1986] "Solution of the implicitly discretised fluid flow equations by operator-splitting," *J. Comput. Phys.* **62**, 40–65.

Noack, R. W., Boger, D. A., Kunz, R. F. and Carrica, P. M. [2009] "Suggar++: An improved general overset grid assembly capability," *Proc. 47th AIAA Aerospace Science and Exhibit*, pp. 22–25.

Pope, S. B. [2000] *Turbulent Flows*, 1st revised edn. (Cambridge University Press), pp. 273–274, ISBN 0-521-59125-2.

Shen, Z., Zhao, W., Wang, J. and Wan, D. [2014] "Manual of CFD solver for ship and ocean engineering flows: naoe-FOAM-SJTU," Shanghai Jiao Tong University.

Shen, Z., Wan, D. and Carrica, P. M. [2015] "Dynamic overset grids in OpenFOAM with application to KCS self-propulsion and maneuvering," *Ocean Eng.* **108**, 287–306.

Shen, Z. and Wan, D. [2016] "An irregular wave generating approach based on naoe-FOAM-SJTU solver," *China Ocean Eng.* **30**, 177–192.

Stern, F., Wilson, R. and Shao, J. [2006] "Quantitative V&V of CFD simulations and certification of CFD codes," *Int. J. Numer. Methods Fluids* **50**, 1335–1355.

Tokyo [2015] A workshop on CFD in ship hydrodynamics, http:// http://www.t2015.nmri.go.jp.

Wang, J., Liu, X. and Wan, D. [2016] "Numerical prediction of KCS self-propulsion in shallow water," *Proc. 26th Int. Offshore and Polar Engineering Conf.*, Rhodes, Greece, pp. 757–763.

Wang, J., Zhao, W. and Wan, D. [2016] "Free maneuvering simulation of ONR Tumblehome using overset grid method in naoe-FOAM-SJTU," *Proc. 31st Symp. Naval Hydrodynamics*, Monterey, USA.

Wang, J., Zou, L. and Wan, D. [2017] "CFD simulations of free running ship under course keeping control," *Ocean Eng.* **141**, 451–464.

Van Leer, B. [1979] "Towards the ultimate conservative difference scheme. V. A second-order sequel to Godunov's method," *J. Comput. Phys.* **32**, 101–136.

Xing, T., Carrica, P. and Stern, F. [2008] "Computational towing tank procedures for single run curves of resistance and propulsion," *J. Fluids Eng.* **130**, 101102.

Zha, R., Ye, H. and Wan, D. [2015] "Numerical computations of resistance of high speed catamaran in calm water," *J. Hydrodyn. Ser. B* **26**, 930–938.